

## PHASE-SPACE ANALYSIS OF FRAGMENTS FORMED IN HEAVY-ION COLLISIONS

*Sakshi Gautam<sup>a</sup>, Preeti Bansal<sup>b</sup>*

<sup>a</sup> Dev Samaj College for Women, Sector 45 B Chandigarh-160047, India

<sup>b</sup> Department of Physics, Panjab University, Chandigarh-160014, India

We study the effect of momentum-dependent interactions and a broader Gaussian on multifragmentation. We also look into the details of the fragment structure for a broader Gaussian and momentum-dependent interactions. We find that nucleons forming the fragments belong to the same region of the phase space.

Мы рассматриваем эффекты импульс-зависимого взаимодействия и гауссовского распределения в мультифрагментации. Мы также изучаем в деталях структуру фрагментов для гауссовского распределения и импульс-зависимого взаимодействия. Мы нашли, что нуклоны, сформированные из фрагментов, принадлежат одной и той же области в фазовом пространстве.

PACS: 25.70.Pq

### INTRODUCTION

The heavy-ion experiments at intermediate energies served as the only candidate to produce hot and compressed nuclear matter in laboratory, one started to hope that these could serve to determine the nuclear matter equation of state, i.e., the dependence of the energy per nucleon on the density and temperature, which is the ultimate goal of heavy-ion collision studies. The nuclear matter equation of state is not only of fundamental importance to the nuclear physics community but it is also essential for astrophysics as it sheds light on the structure of formation of neutron stars and supernova explosions. Since a heavy-ion reaction is a unique way to produce the piece of hot and compressed nuclear matter in laboratory, the heavy-ion experiments started to nourish the hope that they could serve to determine the equation of state of nuclear matter. The breaking of colliding nuclei into fragments of different sizes has been studied for quite a long time. The detailed experimental and theoretical studies revealed that the fragmentation is a complex process that depends crucially on the reaction inputs like the bombarding energy as well as impact parameter [1–4]. Various experimental studies offer a unique opportunity to explore the mechanism behind breaking of nuclei into pieces. At the same time, heavy-ion reaction can also be used to extract information about the nature of the matter. Some processes like kaon production [5,6] give signal about the softer nature of the matter, whereas others give indication that matter could be stiffer in nature. It is also well accepted that the static equation of state (EOS) cannot describe the heavy-ion reaction adequately. The fate of a reaction depends not only on the density, but also on the momentum

space. Therefore, the momentum-dependent interactions play a crucial role in the dynamics of a heavy-ion collision. The momentum-dependent interactions (MDI) are found to affect the collective flow drastically [7–9]. Due to the reduction in the nucleon–nucleon collisions with MDI, the subthreshold particle production is also reduced [7] significantly. Some studies are also reported in the literature that focuses on the effect of MDI on multifragmentation [10]. These studies predicted a significant effect of MDI on multifragmentation. These effects were more pronounced at peripheral collisions. Unfortunately, no study has been carried out to look into the details of the fragment structure using momentum-dependent interactions. One is interested to understand whether fragments are produced due to coalescence or emerge from the particular region of the phase space.

In addition, interaction range has also a major role to play in the dynamics of heavy-ion collisions [11–15]. It has a pronounced effect on the collective flow and on its disappearance, as well as on multifragmentation [11, 12]. For example, in [12] it has been shown that for a broader Gaussian (larger interaction range), the energy of disappearance of flow increases. Similarly, there is a significant effect of interaction range on the fragmentation as well. In [11] it has been shown that a broader Gaussian leads to reduced fragments. But the details of fragment structure for a broader Gaussian was never studied. We, therefore, aim to address

1. The effect of MDI on the fragment structure.
2. The effect of interaction range and to look if fragments then produced belong to certain space or just produced in the reaction without pre-selection.

This study is carried out within the framework of Quantum Molecular Dynamics (QMD) model.

## 1. THE MODEL

We describe the time evolution of a heavy-ion reaction within the framework of Quantum Molecular Dynamics (QMD) model [7] which is based on a molecular dynamics picture. Here each nucleon is represented by a coherent state of the form

$$\psi_i(\mathbf{r}, \mathbf{p}_i(t), \mathbf{r}_i(t)) = \frac{1}{(2\pi L)^{3/4}} \exp \left[ \frac{i}{\hbar} \mathbf{p}_i(t) \cdot \mathbf{r} - \frac{(\mathbf{r} - \mathbf{r}_i(t))^2}{4L} \right], \quad (1)$$

where  $L$  defines the interaction range of the particles. The total  $N$ -body function is assumed to be a direct product of the coherent states (Eq. (1))

$$\Phi = \prod_i \psi_i(\mathbf{r}, \mathbf{r}_i, \mathbf{p}_i, t). \quad (2)$$

By doing this, one neglects the antisymmetrization. One should, however, keep in mind that the Pauli principle, which is very important at low incident energies, has been taken into account. The Wigner transformations of the coherent states are the Gaussians in coordinate and momentum space. The Wigner density reads as

$$f_i(\mathbf{r}, \mathbf{p}, \mathbf{r}_i(t), \mathbf{p}_i(t)) = \frac{1}{(2\pi\hbar)^3} \int e^{-\frac{i}{\hbar} \mathbf{p} \cdot \mathbf{r}_{12}} \psi_i \left( \mathbf{r} + \frac{\mathbf{r}_{12}}{2}, t \right) \psi_i^* \left( \mathbf{r} - \frac{\mathbf{r}_{12}}{2}, t \right) d^3 r_{12}, \quad (3)$$

$$= \frac{1}{(\pi\hbar)^3} \exp \left[ -\frac{(\mathbf{r} - \mathbf{r}_i(t))^2}{2L} \right] \exp \left[ -\frac{(\mathbf{p} - \mathbf{p}_i(t))^2 2L}{\hbar^2} \right]. \quad (4)$$

Here  $\mathbf{r}_i(t)$  and  $\mathbf{p}_i(t)$  define the classical orbit or the center of Gaussian wave packet in phase space. The density of the  $i$ th particle is

$$\begin{aligned}\rho_i(\mathbf{r}) &= \int f_i(\mathbf{r}, \mathbf{p}, \mathbf{r}_i(t), \mathbf{p}_i(t)) d^3p, \\ &= \frac{1}{(2\pi L)^{3/2}} \exp \left\{ \frac{-[\mathbf{r} - \mathbf{r}_i(t)]^2}{2L} \right\}.\end{aligned}\quad (5)$$

The equations of motion for many-body system are then calculated by means of a generalized variational principle. For the coherent states and Hamiltonian of the form  $H = \sum_i T_i + \frac{1}{2} \sum_{ij} V_{ij}$  ( $T_i$  = kinetic energy and  $V_{ij}$  = potential energy), the Lagrangian and the variation can easily be calculated, and we obtain

$$\mathcal{L} = \sum_i \left[ -\dot{\mathbf{r}}_i \mathbf{p}_i - T_i - \frac{1}{2} \sum_{j \neq i} \langle V_{ij} \rangle - \frac{3}{2Lm} \right]. \quad (6)$$

The time evolution of the centroids  $\mathbf{p}_i$  and  $\tilde{\mathbf{r}}_i = \mathbf{r}_i + \mathbf{p}_i t/m$  is given by the Euler-Lagrange equations,

$$\dot{\tilde{\mathbf{r}}}_i = \frac{\mathbf{p}_i}{m} + \nabla_{\mathbf{p}_i} \sum_j \langle V_{ij} \rangle = \nabla_{\mathbf{p}_i} \langle H \rangle, \quad (7)$$

$$\dot{\mathbf{p}}_i = -\nabla_{\mathbf{r}_i} \sum_{j \neq i} \langle V_{ij} \rangle = -\nabla_{\mathbf{r}_i} \langle H \rangle, \quad (8)$$

and  $\langle V_{ij} \rangle = \int d^3\mathbf{r}_1 d^3\mathbf{p}_2 \langle \psi_i^* \psi_j^* | V(\mathbf{r}_1, \mathbf{r}_2) | \psi_i \psi_j \rangle$ . These equations represent the time evolution and can be solved numerically. Therefore, the variational principle reduces the time evolution of  $n$ -body Schrödinger equation to the time evolution  $6 \times (A_P + A_T)$  equation, where  $A_P$  and  $A_T$  represent the mass of projectile and target nuclei. The equations of motion now have a similar structure like the classical Hamiltonian equations

$$\dot{\mathbf{p}}_i = -\frac{\partial \langle H \rangle}{\partial \mathbf{r}_i}, \quad \dot{\mathbf{r}}_i = \frac{\partial \langle H \rangle}{\partial \mathbf{p}_i}. \quad (9)$$

The expectation value of the total Hamiltonian reads

$$\langle H \rangle = \langle T \rangle + \langle V \rangle = \sum_i \frac{\mathbf{p}_i^2}{2m_i} + V^{\text{Skyrme}} + V^{\text{Yuk}} + V^{\text{Coul}} + V^{\text{MDI}}. \quad (10)$$

Here  $V^{\text{Skyrme}}$ ,  $V^{\text{Yuk}}$ ,  $V^{\text{Coul}}$  and  $V^{\text{MDI}}$  are, respectively, the local (two- and three-body) Skyrme, Yukawa, Coulomb and momentum-dependent potentials. The local Skyrme interaction is written as

$$V^{\text{Skyrme}} = \frac{1}{2!} \sum_{j; i \neq j} V_{ij}^{(2)} + \frac{1}{3!} \sum_{j, k; i \neq j \neq k} V_{ijk}^{(3)}. \quad (11)$$

Here  $V_{ij}^{(2)}$  and  $V_{ijk}^{(3)}$  represent, respectively, the two- and three-body interactions. The two-body interactions  $V_{ij}^{(2)}$  are obtained by folding the two-body potential with the densities of

both the nucleons,

$$\sum_{j:i \neq j} V_{ij}^{(2)} = \sum_{j:i \neq j} \int f_i(\mathbf{r}_i, \mathbf{p}_i, t) f_j(\mathbf{r}_j, \mathbf{p}_j, t) V(\mathbf{r}_i, \mathbf{r}_j) d^3 r_i d^3 r_j d^3 p_i d^3 p_j. \quad (12)$$

The three-body interactions can be calculated as follows:

$$\sum_{j,k:i \neq j \neq k} V_{ijk}^{(3)} = \sum_{j,k:i \neq j \neq k} \int f_i(\mathbf{r}_i, \mathbf{p}_i, t) f_j(\mathbf{r}_j, \mathbf{p}_j, t) f_k(\mathbf{r}_k, \mathbf{p}_k, t) V(\mathbf{r}_i, \mathbf{r}_j, \mathbf{r}_k) \times \quad (13)$$

$$\times d^3 r_i d^3 r_j d^3 r_k d^3 p_i d^3 p_j d^3 p_k. \quad (14)$$

The finite-range Yukawa ( $V^{\text{Yuk}}$ ) and effective Coulomb potentials ( $V^{\text{Coul}}$ ) read as

$$V^{\text{Yuk}} = \sum_{j:i \neq j} t_3 \frac{\exp(-|\mathbf{r}_i - \mathbf{r}_j|/\mu)}{|\mathbf{r}_i - \mathbf{r}_j|/\mu}, \quad (15)$$

$$V^{\text{Coul}} = \sum_{j:i \neq j} \frac{Z_{\text{eff}}^2 e^2}{|\mathbf{r}_i - \mathbf{r}_j|}. \quad (16)$$

The Yukawa term (with  $t_3 = -6.66$  MeV and  $\mu = 1.5$  fm) has been added to improve the surface properties of the interaction which plays an important role in fusion and cluster radioactivity [16]. In nuclear matter where the density is constant, the interaction density coincides with the single-particle density, and the two-body Skyrme as well as Yukawa interactions are directly proportional to  $(\rho/\rho_0)$ . The three-body part of the Skyrme interaction is proportional to  $(\rho/\rho_0)^2$ . In nuclear matter, the local potential energy has the form

$$V^{\text{Skyrme}} = \frac{\alpha}{2} \left( \frac{\rho}{\rho_0} \right) + \frac{\beta}{\gamma + 1} \left( \frac{\rho}{\rho_0} \right)^2. \quad (17)$$

The above potential has two free ( $\alpha$  and  $\beta$ ) parameters, which can be fixed by the requirement that at normal nuclear matter density, the average binding energy should be  $-15.75$  MeV and total energy should have a minimum at  $\rho_0$ . In order to investigate the influence of different compressibilities  $K \left[ = 9\rho^2 \frac{\partial^2}{\partial \rho^2} \left( \frac{E}{A} \right) \right]$ , the above potential energy (Eq. (17)) can be generalized to

$$V^{\text{Skyrme}} = \frac{\alpha}{2} \left( \frac{\rho}{\rho_0} \right) + \frac{\beta}{\gamma + 1} \left( \frac{\rho}{\rho_0} \right)^\gamma. \quad (18)$$

This equation leads to the nuclear matter equation of state which connects the pressure and energy. By varying the parameter  $\gamma$ , one can study different equations of state. Naturally, larger value of  $\gamma$  leads to hard equation of state, whereas smaller value of  $\gamma$  results in soft equation of state. The relativistic effect does not play role in low incident energy of present interest [17].

The phase space of the nucleons is stored at several time steps, and this is clustered using minimum snapping tree method that binds the nucleons if they are closer than 4 fm.

## 2. RESULTS AND DISCUSSION

We simulated the reactions  $^{58}\text{Ni} + ^{58}\text{Ni}$  and  $^{197}\text{Au} + ^{197}\text{Au}$  for 100 MeV/nucleon at central ( $\hat{b} = 0.2$ ) and peripheral ( $\hat{b} = 0.8$ ) colliding geometry. For the present study, we used stiff (Hard), soft (Soft), soft with momentum-dependent interactions (SMD) equations of state. The standard energy-dependent Cugnon cross section is used along with two different Gaussian widths, i.e.,  $L = 1.08 \text{ fm}^2$  ( $L^{\text{norm}}$ ) and  $2.16 \text{ fm}^2$  ( $L^{\text{broad}}$ ).

In Fig. 1, we display the time evolution of mass of heaviest fragment, labeled by  $A^{\text{max}}$ , free nucleons, light charged particles, labeled by LCPs ( $2 \leq A \leq 4$ ) and intermediate mass fragments, labeled by IMFs ( $5 \leq A \leq A_{\text{tot}}/6$ , where  $A_{\text{tot}} = A_P + A_T$ ) for the reaction  $^{58}\text{Ni} + ^{58}\text{Ni}$  at  $\hat{b} = 0.2$  and incident energy of 100 MeV/nucleon. The purpose of showing different mass windows is to identify the different phenomena that may appear in one window but not in other mass range. The  $A^{\text{max}}$  will give a possibility to look for the fusion (if any), whereas the emission of free nucleons will show the disassembly and hence vaporization of the nuclear matter. For the central collision of  $\hat{b} = 0.2$  (blue lines), we see from Fig. 1, *a* that  $A^{\text{max}}$  first increases with time, reaches maximum (about 116 which is  $A^{\text{projectile}} + A^{\text{target}}$ ) at about 20–40 fm/c when the matter is highly compressed and then decreases during the later stages at about 120 fm/c. The effect of EOS is negligible on  $A^{\text{max}}$  (solid and dashed lines) as predicted in [2]. From Figs. 1, *b*, *c*, and *d*, we find that free nucleons, LCPs, and IMFs increase with time. This is because the excited compound nucleus decays by the emission of nucleons and fragments. As a result, free nucleons, LCPs, and IMFs display a constant rise in their multiplicities. The constant emission of free nucleons with time suggests that

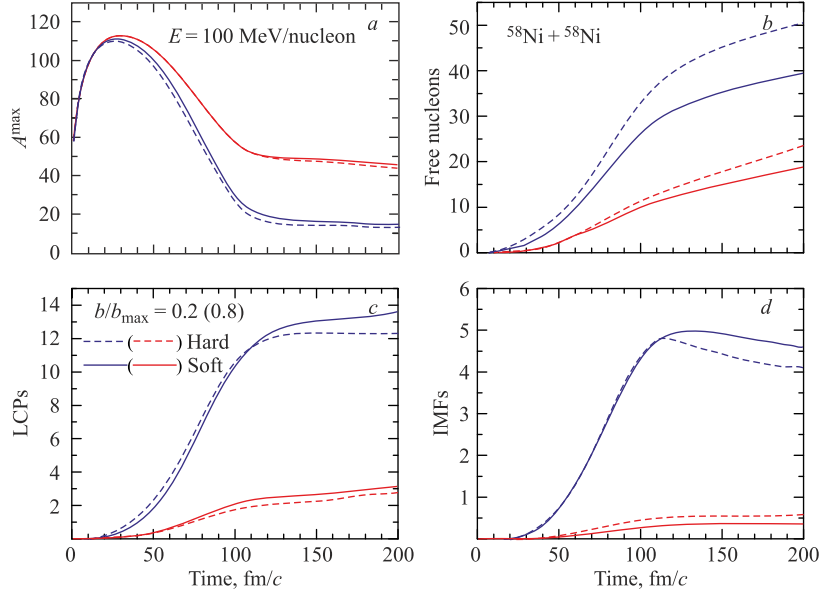


Fig. 1. (Color online) The time evolution of  $A^{\text{max}}$ , free nucleons, LCPs and IMFs for the reaction  $^{58}\text{Ni} + ^{58}\text{Ni}$  at an incident energy of 100 MeV/nucleon at central ( $\hat{b} = 0.2$ ) and peripheral ( $\hat{b} = 0.8$ ) colliding geometry for Soft and Hard EOS. Lines are explained in the text

hot fragments are cooling down. The emission of free nucleons, LCPs, and IMFs starts at around 50 fm/c. We also find a significant effect of EOS on the production of free nucleons, LCPs, and IMFs. We find that the number of LCPs/IMFs is larger in the case of soft EOS compared to hard EOS (see blue and red lines). This is because of the fact that soft matter can be easily compressed. As a result, a greater density can be achieved, which in turn leads to the large number of IMFs compared to that in hard case.

For the peripheral collision of  $\hat{b} = 0.8$  (red lines), we find that  $A^{\max}$ , free nucleons, and LCPs show similar behavior as that for central collision except that the number of free nucleons and LCPs are now significantly reduced. This is because of the fact that less density is achieved in peripheral collisions and, therefore, the number of IMFs is also greatly reduced in peripheral collisions (for both soft and hard EOS) as the static soft and hard EOS are not able to break the initial correlations among the nucleons and hence no IMFs are emitted.

In Fig. 2, we display the effect of momentum-dependent interactions on the production of  $A^{\max}$ , free nucleons, LCPs, and IMFs at  $\hat{b} = 0.2$  and 0.8. We find that  $A^{\max}$  is nearly the same for Soft and SMD (solid and dotted line) at central collisions, whereas the difference increases at peripheral collisions. This is because in central collisions, the nucleon–nucleon collisions are more frequent, which results in complete destruction of the initial correlations. Therefore, an additional repulsion (due to MDI) does not alter the results. We also see that the number of free nucleons and LCPs increases with momentum-dependent interactions due to additional destruction of the remaining correlations (at both central and peripheral collisions). On the other hand, the role of MDI in peripheral collisions is dominant. This is because in the production of IMFs, the additional MDI breaks the heavy fragments into larger number of intermediate mass fragments leading to a lot of IMFs.

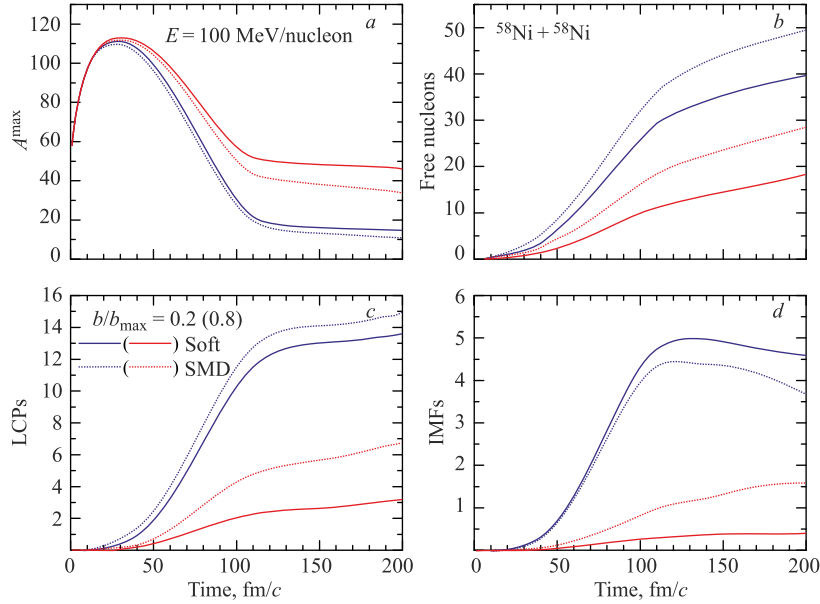
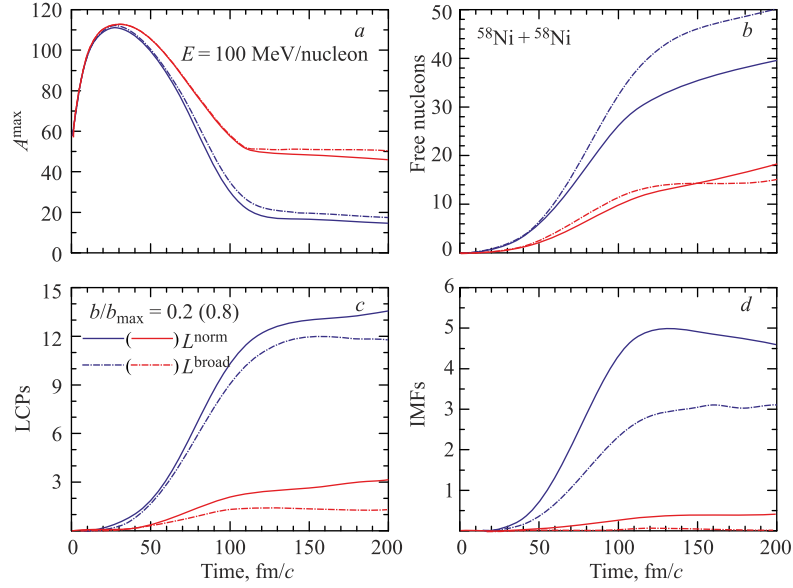
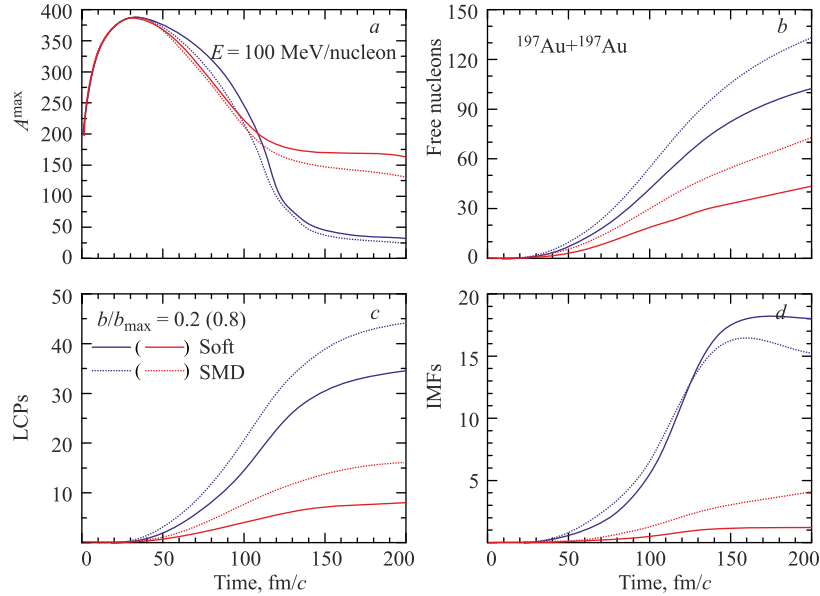


Fig. 2. Same as Fig. 1, but for Soft and SMD


 Fig. 3. Same as Fig. 1, but for  $L^{\text{norm}}$  and  $L^{\text{broad}}$ 

In Fig. 3, we display the effect of interaction range on the production of  $A^{\text{max}}$ , free nucleons, LCPs, and IMFs by using two different widths of Gaussian, that is,  $L^{\text{norm}}$  ( $4.33 \text{ fm}^2$ ) and  $L^{\text{broad}}$  ( $8.66 \text{ fm}^2$ ). We find that the width of Gaussian has a considerable impact on fragmentation. As we change the Gaussian width ( $L$ ) from  $4.33$  to  $8.66 \text{ fm}^2$ , the multiplicity


 Fig. 4. Same as Fig. 2, but for the reaction  $^{197}\text{Au} + ^{197}\text{Au}$

of IMFs is greatly reduced. Owing to its largest interaction range, an extended wave packet ( $L^{\text{broad}}$ ) connects a large number of nucleons in a fragment and as a result it generates heavier fragments compared to what is obtained with a smaller width. It is worth mentioning here that the width of the Gaussian has a considerable effect on the collective flow as well as on the pion production [12–15].

In Fig. 4 we display the effect of MDI on the reactions  $^{197}\text{Au} + ^{197}\text{Au}$  at  $\hat{b} = 0.2$  and 0.8 for 100 MeV/nucleon. A similar behavior of all the quantities is obtained as that for the reaction  $^{58}\text{Ni} + ^{58}\text{Ni}$ . From Fig. 4, we see that now  $A^{\text{max}}$  reaches a maximum value (394) which is the total mass of the system at the highly dense phase of the reaction. Moreover, the number of free nucleons, LCPs, and IMFs are also increased as that in case of  $^{58}\text{Ni} + ^{58}\text{Ni}$  reaction due to increase in the system mass. From Fig. 4 we also see that the number of IMFs

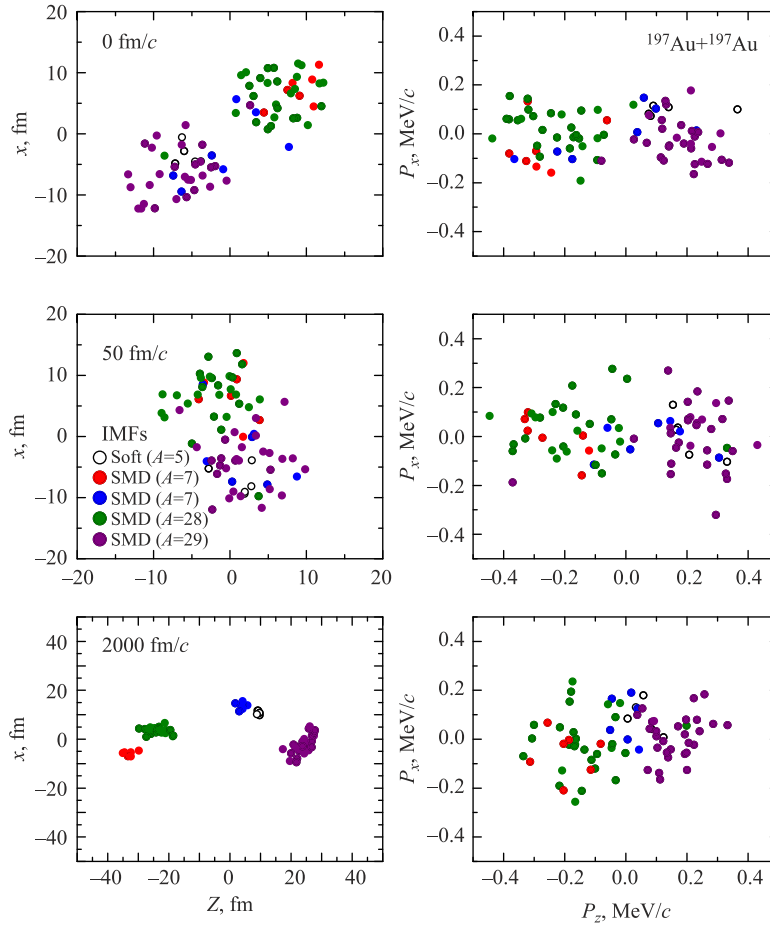


Fig. 5. (Color online) The phase space of the nucleons forming the fragments (IMFs) in the reaction  $^{197}\text{Au} + ^{197}\text{Au}$  with Soft and SMD EOS at 0 (top panels), 50 (middle) and 200 (bottom) fm/c. Symbols are explained in the text

is larger in case of SMD than that in case of Soft (static) EOS because of the destruction of initial correlations due to the repulsive momentum-dependent interactions as discussed previously. We further investigate the details of the fragments formed in static and MDI interactions.

In Fig. 5, we display the phase space of those nucleons which form IMFs in case of Soft and SMD EOS at initial time, i.e., 0 fm/c (top panels), at intermediate stage at 50 fm/c (middle panels) and at the end of reaction at 200 fm/c (bottom panels). Left (right) panels display the coordinate (momentum) space. Solid (open) circles represent SMD (Soft) EOS. From the figure, we see that nucleons forming an IMF in case of Soft EOS belong to the same region of coordinate space (see open circles). In case of MDI also, most of the nucleons which form the IMFs are coming from the same region (closed circles).

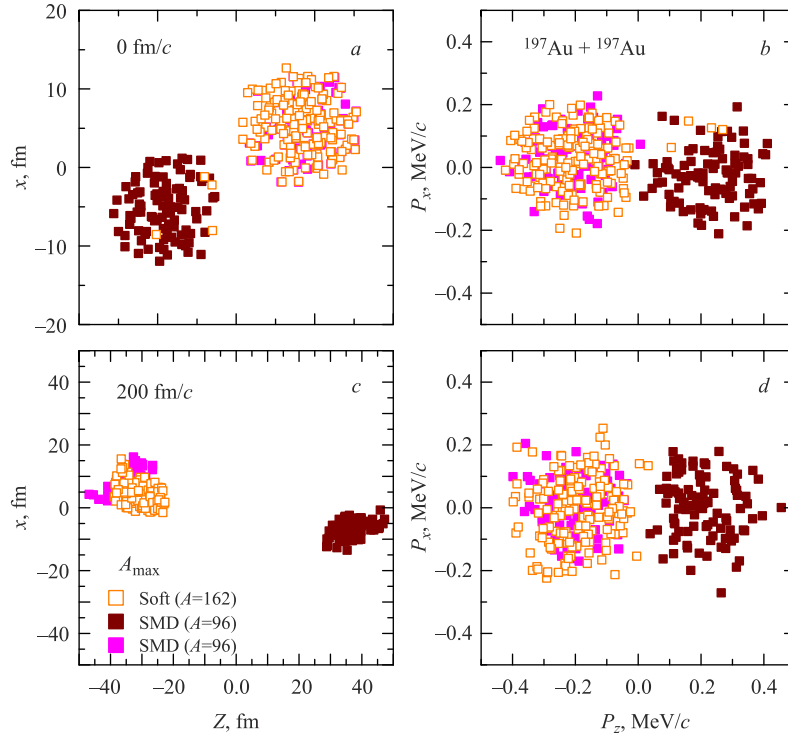


Fig. 6. Same as Fig. 5, but for the  $A^{\max}$  formed with Soft and SMD EOS at 0 (a, b) and 200 (c, d) fm/c

In Fig. 6, we display the phase space of the nucleons forming the  $A^{\max}$  in case of Soft and SMD EOS. We see that for the formation of  $A^{\max}$ , the participating nucleons belong to the same region of phase space. We also see that  $A^{\max}$  in case of SMD is small as compared to that in case of static one.

In Fig. 7, we display the effect of interaction range on the production of  $A^{\max}$ , free nucleons, LCPs, and IMFs by using two different widths of Gaussian, that is,  $L^{\text{norm}}$  ( $4.33 \text{ fm}^2$ ) and  $L^{\text{broad}}$  ( $8.66 \text{ fm}^2$ ) for the reaction  $^{197}\text{Au} + ^{197}\text{Au}$ . We find the similar effect of interaction range of the fragment production as for the reaction  $^{58}\text{Ni} + ^{58}\text{Ni}$ , i.e., with broader Gaussian,

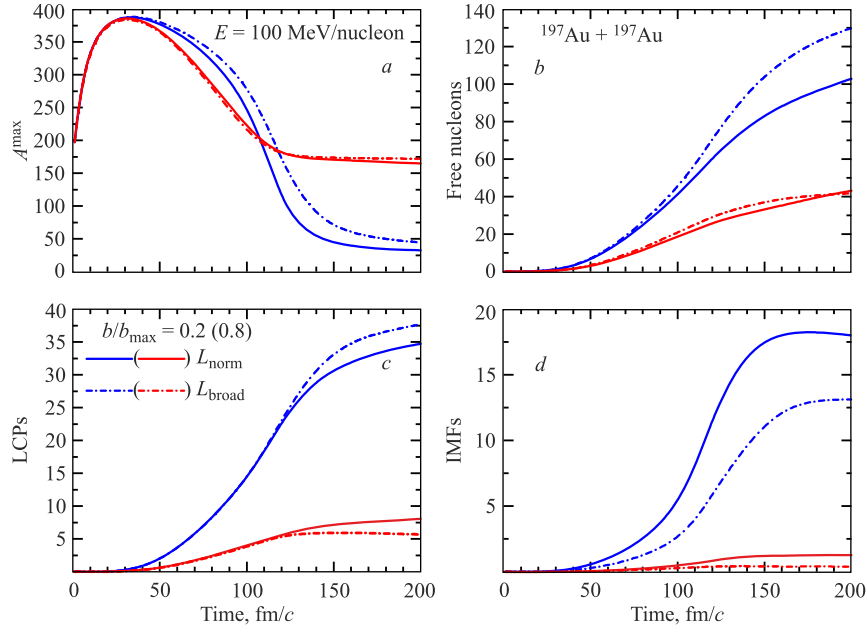


Fig. 7. Same as Fig. 3, but for the reaction  $^{197}\text{Au} + ^{197}\text{Au}$

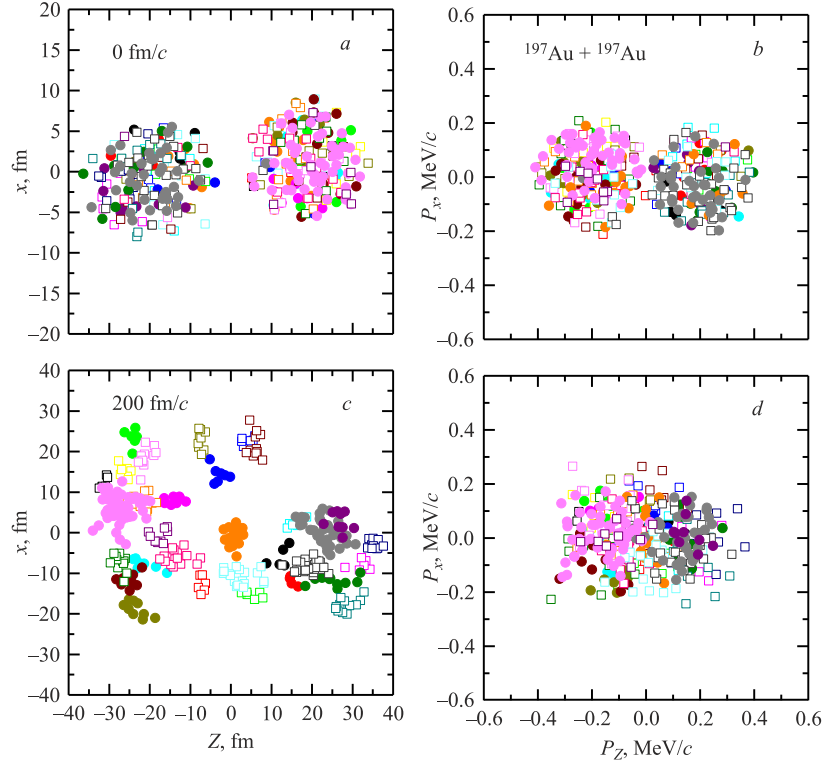


Fig. 8. The phase space of the nucleons forming the fragments (IMFs) in the reaction  $^{197}\text{Au} + ^{197}\text{Au}$  with  $L^{\text{norm}}$  and  $L^{\text{broad}}$  at 0 (a,b) and 200 (d,c) fm/c. Solid (open) symbols are for  $L^{\text{broad}}$  ( $L^{\text{norm}}$ )

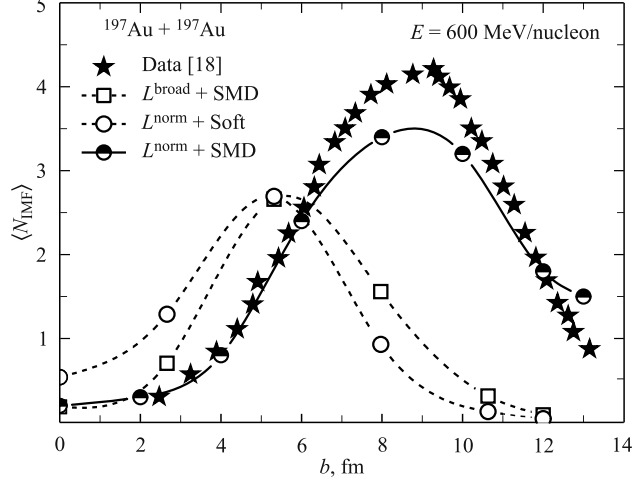


Fig. 9. The mean IMF multiplicity  $\langle N_{\text{IMF}} \rangle$  vs. the impact parameter for the reaction  $^{197}\text{Au} + ^{197}\text{Au}$  at an incident energy of 600 MeV/nucleon. Various symbols are explained in text

the IMFs production is reduced. To have a further insight into the fragment structure, that is, whether the nucleons forming a fragment when we increase the interaction range belong to the same region of phase space or not, in Fig. 8, we display the phase space of the nucleons which are forming the IMFs with both  $L^{\text{norm}}$  and  $L^{\text{broad}}$  at 0 and 200 fm/c. We find that the nucleons which are forming the fragment belong to the same region of phase space.

As a final step, we compare the model calculations with the experimental data [18] for the reaction  $^{197}\text{Au} + ^{197}\text{Au}$  at 600 MeV/nucleon (Fig. 9). Stars represent the data. Circles and half shaded circles represent the calculations for normal Gaussian width ( $L^{\text{norm}}$ ) with Soft and SMD EOS, respectively. Squares represent the calculations for  $L^{\text{broad}}$  with SMD EOS. From the figure, we see that normal Gaussian width along with the SMD EOS best agrees with the experimental data. With Soft EOS, IMF multiplicity increases for nearly central collisions and decreases for peripheral collisions as explained earlier in Fig. 4. Also, with broader Gaussian IMF multiplicity decreases as in Fig. 7.

### 3. SUMMARY

We studied the effect of momentum-dependent interactions and a broader Gaussian on multifragmentation as well as the fragment structure. We find that nucleons forming the fragments belonged to the same region of phase space. A comparison with experimental data also shows the adequacy of the model to the physics of heavy-ion collisions.

### REFERENCES

1. Aichelin J., Stöcker H. // Phys. Lett. B. 1986. V. 176. P. 14.
2. Kumar S. et al. // Phys. Rev. C. 1998. V. 58. P. 320;  
Dhawan J., Puri R. K. // Phys. Rev. C. 2007. V. 75. P. 057601;  
Goyal S. // Phys. Rev. C. 2011. V. 83. P. 047601.

3. *Puri R. K. et al. // Phys. Rev. C. 1996. V. 54. P. 28;*  
*Puri R. K. et al. // Phys. Rev. C. 1998. V. 57. P. 2744;*  
*Puri R. K., Aichelin J. // J. Comp. Phys. 2000. V. 162. P. 245.*
4. *Williams C. et al. // Phys. Rev. C. 1997. V. 55. P. R2132;*  
*Tsang M. B. et al. // Phys. Rev. Lett. 1993. V. 71. P. 1502;*  
*Vermani Y. K. et al. // Phys. Rev. C. 2009. V. 79. P. 064613.*
5. *Hartnack C., Oeschler H., Aichelin J. // Phys. Rev. Lett. 2006. V. 96. P. 012302.*
6. *Fuchs C. et al. // Phys. Rev. Lett. 2001. V. 86. P. 1974;*  
*Huang S. W. et al. // Phys. Lett. B. 1998. V. 298. P. 41;*  
*Huang S. W. et al. // Prog. Nucl. Part. Phys. 1993. V. 30. P. 105;*  
*Batko G. et al. // J. Phys. G: Nucl. Part. Phys. 1994. V. 20. P. 461.*
7. *Aichelin J. // Phys. Rep. 1991. V. 202. P. 233.*
8. *Aichelin J. et al. // Phys. Rev. Lett. 1987. V. 58. P. 1926.*
9. *Sood A. D., Puri R. K. // Eur. Phys. J. A. 2006. V. 30. P. 571;*  
*Kumar S., Puri R. K. // Phys. Rev. C. 2008. V. 78. P. 064602;*  
*Singh J., Kumar S., Puri R. K. // Phys. Rev. C. 2001. V. 63. P. 054603;*  
*Kumar S., Puri R. K. // Phys. Rev. C. 1999. V. 60. P. 054607;*  
*Chugh R., Puri R. K. // Phys. Rev. C. 2010. V. 82. P. 014603.*
10. *Peilert G. et al. // Phys. Rev. C. 1989. V. 39. P. 1402.*
11. *Hartnack C. et al. // E. Phys. J. A. 1998. V. 1. P. 151.*
12. *Gautam S. et al. // J. Phys. G: Nucl. Part. Phys. 2010. V. 37. P. 085102;*  
*Gautam S. et al. // Phys. Rev. C. 2011. V. 82. P. 014604;*  
*Gautam S. et al. // Ibid. V. 83. P. 014603.*
13. *Hartnack C. et al. // Nucl. Phys. A. 1994. V. 580. P. 643.*
14. *Klakow D., Welke G., Bauer W. // Phys. Rev. C. 1993. V. 48. P. 1982.*
15. *Hartnack C. et al. // Nucl. Phys. A. 1994. V. 580. P. 643.*
16. *Puri R. K. et al. // J. Phys. G: Nucl. Part. Phys. 1992. V. 18. P. 903;*  
*Puri R. K. et al. // Ibid. P. 1533;*  
*Puri R. K. et al. // Eur. Phys. J. A. 1998. V. 3. P. 277.*
17. *Lehmann E. et al. // Phys. Rev. C. 1995. V. 51. P. 2113;*  
*Lehmann E. et al. // Prog. Part. Nucl. Phys. 1993. V. 30. P. 219.*
18. *Schüttauf A. et al. // Nucl. Phys. A. 1996. V. 607. P. 457.*

Received on May 20, 2012.